Research Square

Preprints are preliminary reports that have not undergone peer review.
They should not be considered conclusive, used to inform clinical practice,
or referenced by the media as validated information.

A state-resolved Hawking channel for an area-law quantum memory

Shalender Singh

singhshalender@gmail.com

Independent Researcher https://orcid.org/0000-0003-3677-4043

Vishnu Priya Singh Parmar

Independent Researcher

Article

Keywords:

Posted Date: August 6th, 2026

DOI: https://doi.org/10.21203/rs.3.rs-10556243/v1

License: This work is licensed under a Creative Commons Attribution 4.0 International License.
Read Full License

Additional Declarations: The authors declare no competing interests.

A state-resolved Hawking channel for an area-law quantum memory

Abstract

Black-hole evaporation can be unitary only if Hawking's thermal spectrum is a coarse view of an underlying pure quantum process. Island and replica-wormhole calculations recover the Page curve but do not generally provide the amplitudes mapping a specified black-hole microstate to outgoing quanta. Here we construct such a state-resolved channel for an area-law quantum memory in matrix black-hole quantum mechanics. An exact symmetry separates the fermionic state into a geometric factor that controls emission and a protected factor untouched by the full real- and imaginary-time matrix and link dynamics. We prove that this memory occurs in every representation sector, enumerate all sectors through rank ten, and exhibit a self-complementary sector whose entropy scales with horizon area. When the matrix rank decreases, an exact branching isometry transfers the memory into daughter-hole and radiation degrees of freedom. Combining this isometry with the model's monopole-tunnelling weights gives every encoded state the same Hawking-thermal branch probabilities while its conditional radiation remains pure and microstate dependent. Finite-rank simulations show Page-like transfer and near-unit decoding; dephasing leaves the branch probabilities unchanged but erases recovery. The result provides an explicit amplitude-level mechanism by which Hawking thermality and unitary information transfer coexist in one microscopic model.

From a Page curve to amplitudes

A thermal spectrum is a probability distribution, not a wavefunction. Hawking's calculation determines the probabilities of outgoing quanta seen by a coarse observer, whereas unitary evaporation requires the complete set of amplitudes that maps each initial black-hole microstate into a distinct pure radiation state[1]. A pure many-body state can look thermal when only a small set of observables is measured. The information paradox asks whether a microscopic black-hole dynamics can produce that separation rather than merely assume it.

The Page curve is a decisive consistency test. Islands and replica wormholes reproduce the unitary entropy curve and identify when the radiation entanglement wedge includes an interior region[2–4]. These calculations determine an entropy rather than, in general, the amplitude-level map

$$|I\rangle_{\mathrm{BH}} \longmapsto \sum_{n,B,R} \mathcal{A}^{(n)}_{B,R\leftarrow I} |N-n,B\rangle_{\mathrm{BH}} |n,R\rangle_{\mathrm{rad}}, \tag{1}$$

for a specified microscopic Hamiltonian. Those amplitudes determine where an infalling qubit is encoded, whether it can be decoded, and whether an interior partner can be reconstructed. Entropy alone cannot answer these state-by-state questions.

Matrix black-hole quantum mechanics provides a concrete place to look. In the model of Ref. [5], a rank-N fuzzy sphere and a half-filled fermion sea reproduce Schwarzschild and area-law scaling. Its rank-changing extension derives a monopole tunnelling branch with a Boltzmann probability at the Hawking temperature and explicitly leaves the emitted multipartite wavefunction open[6]. A two-block completion adds an exterior matrix sector, physical bifundamental links and a Gauss constraint on the combined system[7].

Here we construct this open wavefunction on a broad family of protected sectors and give a closed-form area-law example. The key is an exact symmetry of the fermion coupling: the geometry acts on one matrix index and leaves the other untouched. That untouched index stores a protected quantum memory. Rank loss does not erase this memory; an exact representation-theoretic branching rule reroutes it into daughter and radiation degrees of freedom. The tunnelling saddle fixes the common thermal weight, whereas the branching amplitudes retain the state. The result is derived from one matrix Hamiltonian, without a random evaporation circuit or an ensemble of Hamiltonians.

Protection is broad, not isolated

Each matrix fermion carries a spin label and two matrix labels. The black-hole coordinates and the horizon–environment links act on the spin and row label, but not on the terminal column label[7]. If $A_N = \mathbb{C}^2 \otimes \mathbb{C}^N$ denotes the active spin–row space and $F_N = \mathbb{C}^N$ the untouched column space, then every real-, Euclidean- or closed-time field history Φ acts as

$$U_F[\Phi] = \bigwedge^{N^2} (U_A[\Phi] \otimes \mathbf{1}_{F_N}) \,. \tag{2}$$

The column combinations therefore behave as a quantum memory that is invisible to the entire bosonic trajectory.

Skew–Howe duality makes this memory explicit[8, 9]. At half filling,

$$\mathcal{C}_N = \bigwedge^{N^2} (A_N \otimes F_N) \cong \bigoplus_{\lambda \vdash N^2} S_\lambda A_N \otimes S_{\lambda^\intercal} F_N, \tag{3}$$

and the evolution acts only on the first factor of every summand,

$$U_F[\Phi]\big|_\lambda = S_\lambda(U_A[\Phi]) \otimes \mathbf{1}_{S_{\lambda^\intercal} F_N}. \tag{4}$$

The second factor is therefore a protected subsystem, or quantum memory, in *every* allowed representation sector. The theorem is not tied to one selected state space. To quantify how broadly protection is distributed, we exactly enumerated all partitions of N^2 inside the allowed $N \times 2N$ rectangle through $N = 10$. At $N = 10$, sectors carrying 71.5% of the total half-filled state count have a protected entropy of at least 30% of the full entropy; the state-weighted median is 31.2% (Extended Data Fig. 5). Thus area-law protection is a structural feature of the full decomposition, not an isolated algebraic accident.

For a closed-form code we choose the distinguished self-complementary highest weight

$$\mu^{(N)} = (2N-1, 2N-3, \ldots, 1), \qquad \mu_i + \mu_{N+1-i} = 2N, \qquad \lambda = (\mu^{(N)})^\intercal, \tag{5}$$

which is invariant under complementing occupied and empty cells in the half-filled $N \times 2N$ rectangle and has uniform adjacent spacing. For this sector the Weyl formula gives the exact dimension

$$\boxed{\dim \mathcal{Q}_N = 3^{N(N-1)/2}.} \tag{6}$$

Symmetry-protected horizon sectors have been proposed before[10], but here the protected factor follows from a specified interaction algebra and is carried through a rank-changing evaporation branch. Its entropy grows as N^2, the same area scaling as the matrix black-hole entropy. More precisely,

$$S_{\text{protected}} = \frac{N(N-1)}{2} \ln 3 = \frac{\ln 3}{4 \ln 2} \, S_{\text{model}} + O(N), \tag{7}$$

so the exact protected sector carries 39.62% of the leading entropy coefficient. At $N = 10$ it lies above 81.7% of all sectors by protected dimension and approaches the upper edge of the exact census. It is therefore a distinguished, near-maximal witness of a protection mechanism that is present sector by sector.

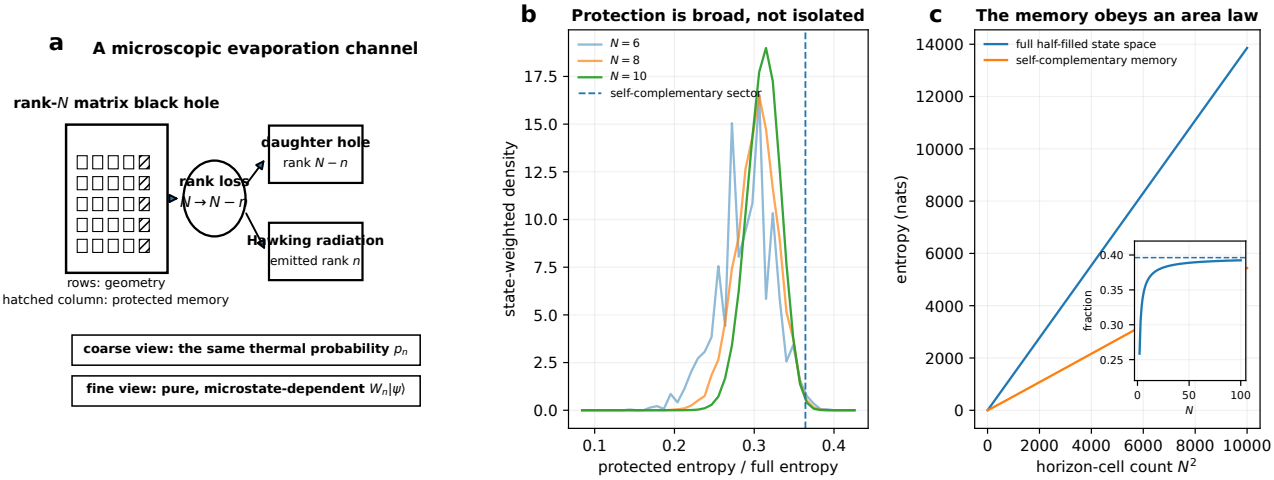


Figure 1: **An area-law quantum memory beneath Hawking thermality.** **a**, the geometry acts on the matrix-row index while the terminal column index stores protected information. Rank loss opens a physical link and routes that state into daughter-hole and radiation degrees of freedom. **b**, exact enumeration of every allowed representation sector shows that large protected factors are broadly distributed; the dashed line marks the self-complementary sector. **c**, its entropy grows linearly with the horizon-cell count N^2 and approaches the finite fraction $\ln 3/(4\ln 2)$ of the full half-filled entropy. No fit is used.

Rank loss routes the quantum state

Suppose the horizon loses rank n, so that $N \to K = N - n$. The terminal space splits as $F_N = F_K \oplus F_n$. The protected memory must then be re-expressed in daughter and emitted variables. The Littlewood–Richardson branching rule gives exactly

$$S_\mu(F_K \oplus F_n) \cong \bigoplus_{\alpha,\beta} \mathbb{C}^{c^\mu_{\alpha\beta}} \otimes S_\alpha F_K \otimes S_\beta F_n, \tag{8}$$

where the coefficients $c^\mu_{\alpha\beta}$ count the allowed daughter–radiation sectors. Choosing orthonormal bases turns this identity into a unitary information-routing map,

$$\boxed{W_{N\to K,n} : \mathcal{Q}_N \longrightarrow \bigoplus_{\alpha,\beta} \mathbb{C}^{c^\mu_{\alpha\beta}} \otimes \mathcal{Q}_{K,\alpha} \otimes \mathcal{R}_{n,\beta}, \qquad W^\dagger W = \mathbf{1}.} \tag{9}$$

For one-rank emission this is the multiplicity-free Gelfand–Tsetlin branching map[11]. The map is deterministic: the initial logical amplitudes fix the daughter–radiation amplitudes.

The full branch separates into a geometric factor and this protected map,

$$K_{n,\lambda} = B_{n,\lambda} \otimes W_{N\to K,n}. \tag{10}$$

For a fixed initial geometry and a complete final branch,

$$K^\dagger_{n,\lambda} K_{n,\lambda}\big|_{\mathcal{Q}_N} = p_{n,\lambda}\, \mathbf{1}_{\mathcal{Q}_N}. \tag{11}$$

Every protected microstate therefore has the same coarse probability for that branch, although $W_{N\to K,n}|\psi\rangle$ remains different for every input state. The earlier monopole calculation supplies the scalar law

$$P(\omega) = e^{-\omega/T}, \qquad T = \frac{M_P}{3N}, \tag{12}$$

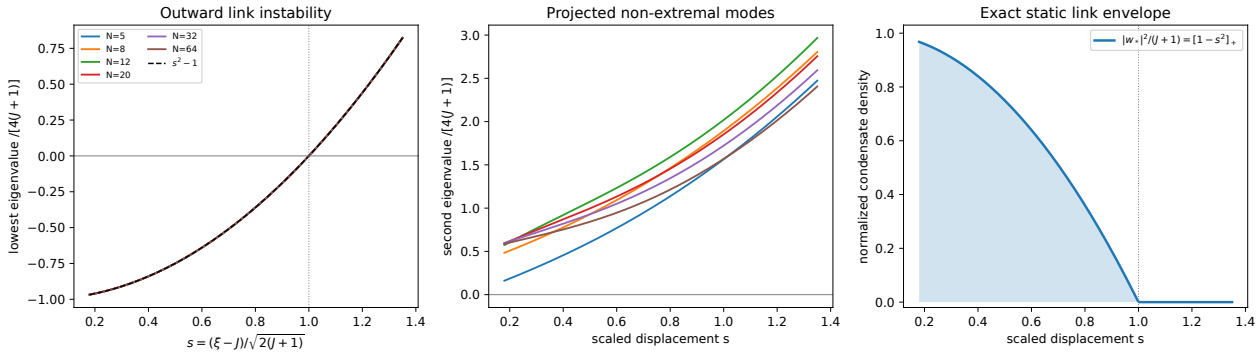


Figure 2: **The matrix dynamics select one outward horizon link. Left**, the lowest transverse Hessian eigenvalue follows the universal instability s^2-1 for every tested rank. **Middle**, the next physical mode stays positive, so the instability is unique in the projected spectrum. **Right**, the quartic interaction stabilizes a finite link condensate with envelope $[1-s^2]_+$. The eigenvalue agreement is better than 1.8×10^{-13}; further numerical details are in Methods and Extended Data.

which has the Hawking $1/N$ scaling and equals $T_H = bM_P/(8N)$ for the parent-model matching $b = 8/3$[6]. That coefficient match is inherited, not a new prediction of this work. Our advance is the operator promotion

$$p_{n,\lambda} \longrightarrow K_{n,\lambda} = \sqrt{p_{n,\lambda}}\, W_{N\to K,n}, \qquad K^\dagger_{n,\lambda} K_{n,\lambda} = p_{n,\lambda}\mathbf{1}_{\mathcal{Q}_N}, \tag{13}$$

which turns the scalar probability into a state-resolved quantum channel. The same microscopic branch is therefore thermal at the level of emitted energy and unitary at the level of the complete state.

A physical link opens at the horizon

The information map is not attached to an arbitrary boundary. In the two-block matrix theory, the outward bifundamental mode becomes unstable only near the fuzzy horizon[7]. Its quadratic eigenvalue is

$$k_-(\xi) = 2(\xi - J)^2 - 4(J+1), \tag{14}$$

and the quartic interaction stabilizes the link with envelope

$$\boxed{|w_*(\xi)|^2 = \left[J + 1 - \frac{1}{2}(\xi - J)^2\right]_+}. \tag{15}$$

We diagonalized the complete fixed-angular-momentum Hessian after projecting onto the background-covariant transverse subspace. For ranks $N = 5$–64, the entire unstable interval contains exactly one physical negative mode, always the outward mode of Eq. (14); all other projected modes remain stable. A reduced Euclidean boundary-value calculation then produces a localized condensate following Eq. (15). The matrix dynamics therefore select both the location and helicity of the horizon–radiation interface.

Thermality without information loss

The elementary branching map can be iterated as the matrix rank decreases. A complete Gelfand–Tsetlin pattern then records one pure evaporation trajectory: its lower rows describe the daughter and the removed rows describe the accumulated radiation. Haar-typical states inside the fixed protected sector show the expected Page-like transfer. The daughter–radiation entropy first rises, peaks when the two sides

have comparable capacity, and returns to zero when the complete pure state has moved into radiation. No random Hamiltonian is used; randomness only samples initial states within one exact code.

We tested information recovery directly. A four-dimensional logical reference was embedded in the $N = 3$ protected sector and decoded from the accumulated radiation with the Petz recovery map[12]. Coherent-radiation recovery rises from the no-information value to near unity and becomes exact after complete emission. The decisive control keeps every coarse rank and energy probability fixed but removes radiation-basis phases. This dephased channel has the same apparent thermality yet loses the ability to distinguish phase-opposite microstates and ends at the complete-dephasing fidelity $1/q$ for a q-dimensional code.

Gauge edges preserve the code

Gauge theories do not factor cleanly across a boundary because the two sides must carry matching charge. The total Gauss law of the black-hole–environment matrix system therefore introduces edge degrees of freedom[7, 13, 14]. If the horizon code decomposes as

$$\mathcal{C}_N = \bigoplus_\rho V_\rho \otimes M_\rho \tag{16}$$

and the edge contains conjugate sectors $V_\rho^* \otimes E_\rho$, then

$$\mathrm{Inv}(\mathcal{C}_N \otimes \mathcal{E}) \cong \bigoplus_\rho M_\rho \otimes E_\rho. \tag{17}$$

Preserving the complete state capacity in each gauge sector requires and is achieved by

$$\boxed{\dim E_\rho \geq \dim V_\rho.} \tag{18}$$

The minimal edge reservoir is therefore fixed by gauge representation theory rather than added as an arbitrary purifier. Exact enumeration through $N = 9$ shows that one conjugate copy per representation loses an exponentially growing fraction of the code, whereas the minimal multiplicity in Eq. (18) restores the state count to numerical precision. Gauge consistency and information capacity point to the same edge structure.

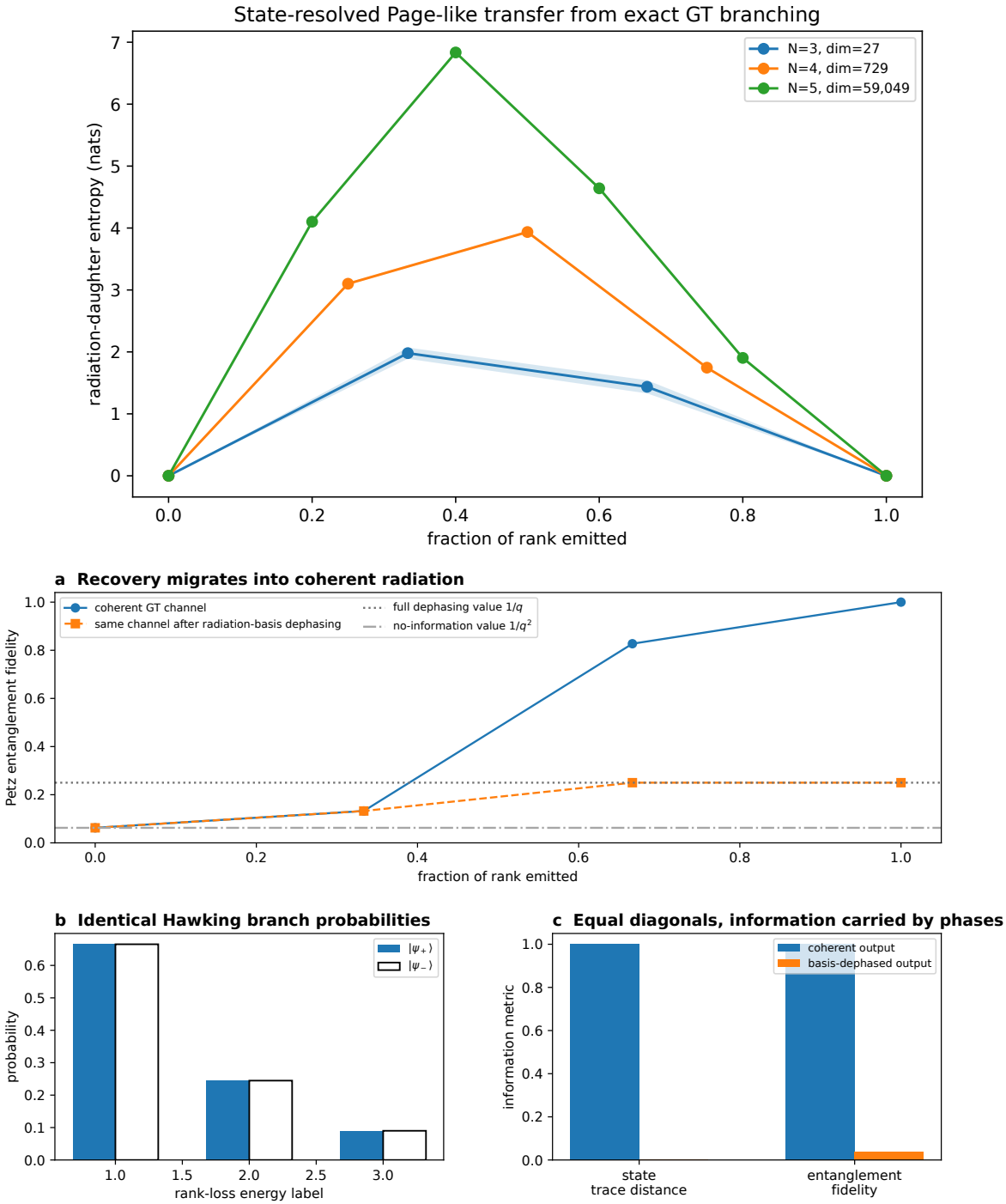


Figure 3: **Information transfer and recovery in the exact branching channel. Top**, typical protected states at ranks $N = 3, 4, 5$ show Page-like daughter–radiation entropy as rank is emitted; the endpoint is pure because all information has moved to radiation. **Bottom**, coherent radiation becomes a high-fidelity carrier of an encoded reference, whereas basis dephasing suppresses recovery. Orthogonal logical states can have identical Hawking branch probabilities and identical populations but remain perfectly distinguishable only when their phases are retained. Shading denotes one standard deviation over sampled pure states.

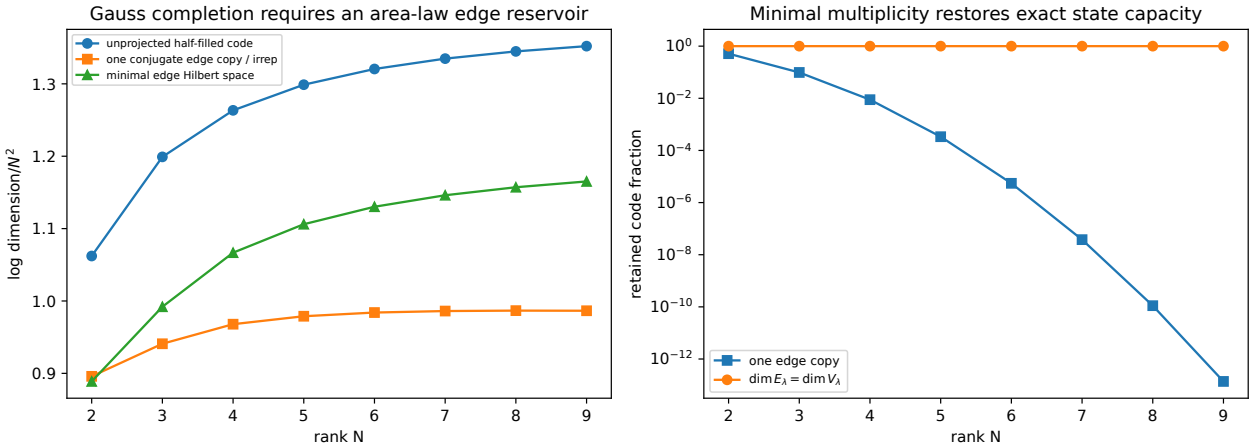


Figure 4: **Gauge consistency requires an area-law edge reservoir. Left**, the half-filled black-hole code, a single-copy gauge completion and the minimal edge Hilbert space all show their distinct large-rank growth. **Right**, one conjugate edge copy per gauge representation retains an exponentially vanishing fraction of the code, whereas the minimal multiplicity $\dim E_\rho = \dim V_\rho$ restores the exact state capacity.

What the channel changes

The result resolves the thermality–unitarity tension for an explicit area-law sector of this matrix model. Hawking thermality is the state-independent probability of a coarse emission branch. Unitarity is carried by the conditional amplitudes inside that branch. The two statements are not competing descriptions: they are different levels of one quantum channel. Unlike a random-circuit evaporation model, the protected memory, its rank-changing map and the physical link that opens the channel all follow from the interaction algebra of a specified matrix Hamiltonian.

This also clarifies what the Page curve leaves open. An entropy curve establishes that enough information returns, but not which radiation amplitudes contain a chosen microstate or how to recover it. Equations (9)–(11) provide those objects for a code whose entropy is proportional to horizon area. The numerical dephasing test then isolates the carrier of the information: changing the phases destroys recovery without changing the thermal branch statistics.

The exact commutant theorem applies sector by sector throughout the half-filled Fock space; what remains sector dependent is the active geometric factor and hence the relative rate between different sectors. The closed-form code in Eq. (6) is a distinguished self-complementary witness, while the exact census shows that large protected memories are widespread. The scalar temperature and its $b = 8/3$ parameter match are inherited from the monopole saddle, whereas the state-resolved isometry is new here. A complete smooth-infall test would additionally require reconstructing an interior partner and verifying its near-horizon correlator. The present result supplies the amplitude-level channel on which those calculations, as well as explicit black-hole error-correction tests, can now be performed.

Methods

Schwinger–Keldysh factorization

On a closed contour C, the fermionic action has the form

$$S_F = \int_C dt \sum_{r=1}^{N} \bar{\psi}_r (i\partial_t - h[\Phi(t)])\psi_r, \tag{19}$$

where r is the terminal column index. The matrix and link fields change the row/block index but leave r unchanged. Hence the contour propagator is $U_A[\Phi] \otimes \mathbf{1}_F$. Second quantization and Eq. (3) give Eq. (4) for each contour history separately. The bosonic measure and action multiply only the geometric operator, so contour integration preserves the identity superoperator on $Q_{\lambda,N}$.

For a fixed initial geometric state $|g\rangle$ and a complete final geometric branch, write the amplitude as $B_{n,\lambda} \otimes W$. Then

$$(K_{n,\lambda}^\dagger K_{n,\lambda})|_{\mathcal{Q}_N} = \langle g|B_{n,\lambda}^\dagger B_{n,\lambda}|g\rangle\, \mathbf{1}_{\mathcal{Q}_N}. \tag{20}$$

No typicality or Haar assumption enters this identity.

Inherited scalar temperature

The parent monopole saddle compares a direct decay from energy E_1 with a decay that first emits a quantum of energy $\omega = E_1 - E_2$. Consistency gives $\Gamma_{E_1} = P(\omega)\Gamma_{E_2}$ and hence $P(\omega) = \exp(-\omega/T)$ with $T = \Omega/(2\pi) = M_P/(3N)$. The Schwarzschild temperature in the same conventions is $T_H = bM_P/(8N)$, so the numerical coefficient agrees for $b = 8/3$[6]. We use this published scalar weight without refitting it. Equations (10) and (11) are the new operator-valued completion.

Odd-staircase dimension and sector census

For $\mu_i = 2(N-i)+1$,

$$\mu_i - \mu_j + j - i = 3(j-i). \tag{21}$$

Every factor in the Weyl product is therefore 3, proving Eq. (6). The Young diagram fits the required rectangle because $\ell(\mu) = N$, $\mu_1 = 2N-1$, and $|\mu| = N^2$. Particle–hole conjugation in this rectangle sends μ_i to $2N - \mu_{N+1-i}$ and therefore fixes the odd staircase exactly. For the census, all bounded partitions of N^2 with at most N rows and row length at most $2N$ were enumerated through $N = 10$. Both Schur dimensions were evaluated by the Weyl formula in logarithmic arithmetic. Their sector-dimension sum reproduces $\binom{2N^2}{N^2}$ with maximum logarithmic error 5.7×10^{-14}.

Branching and Gelfand–Tsetlin numerics

Equation (8) is the standard restriction of a Schur functor to a direct sum. For $n = 1$, daughter highest weights ν satisfy

$$\mu_1 \geq \nu_1 \geq \mu_2 \geq \cdots \geq \nu_{N-1} \geq \mu_N. \tag{22}$$

The odd staircase has gaps of two, so the first rank step exposes 3^{N-1} interlacing rows. Complete Gelfand–Tsetlin patterns were enumerated for $N \leq 5$. To sample a Haar-random state without storing all patterns, each fixed boundary row was represented by a complex Gaussian matrix of size $d_{\text{prefix}} \times d_{\text{daughter}}$, followed by global normalization. Singular values of all blocks give the exact bipartite entropy.

For Petz recovery, a random four-dimensional code was embedded isometrically in the $N = 3$ protected space. The exact pattern split gives Kraus matrices A_j for the radiation channel. For $\rho = \mathbf{1}/q$, the Petz Kraus operators are

$$R_j = q^{-1/2} A_j^\dagger \, [\mathcal{N}(\rho)]^{-1/2}. \tag{23}$$

The plotted quantity is the entanglement fidelity of $\mathcal{R} \circ \mathcal{N}$. Radiation-basis dephasing was applied through projectors before constructing the same recovery map.

Link Hessian and reduced cap

The fixed-M matrices were assembled from the published curl Hessian and spin coupling[7]. In the helicity basis (w_0, w_+, w_-), the transverse condition has coefficients $(M - \xi, A_M, B_M)$, with

$$A_M^2 = \frac{(J+M)(J-M+1)}{2}, \qquad B_M^2 = \frac{(J-M)(J+M+1)}{2}. \tag{24}$$

Each matrix was projected onto the numerical nullspace of this row and diagonalized. The scan used 240 values of s and ranks $N = 5, 8, 12, 20, 32, 64$.

The reduced Euclidean action was

$$I_E[y] = \int d\tau \left[\frac{1}{2}(y')^2 + \frac{1}{2}(s^2-1)y^2 + \frac{1}{4}y^4 \right]. \tag{25}$$

We used $s(\tau) = 1.2[1 - \operatorname{sech}^2(\tau/3)]$ and $y(\pm 15) = 0$. A collocation boundary-value solver converged with maximum rms residual 2.4×10^{-9} and gave $I_E = -1.05535$ relative to the zero configuration.

Gauss-edge enumeration

Bounded partitions of N^2 with at most N rows and row length at most $2N$ were enumerated through $N = 9$. Schur dimensions were evaluated with the hook-content formula in logarithmic arithmetic. If $d_\rho = \dim V_\rho$ and $m_\rho = \dim M_\rho$, the original code dimension is $\sum_\rho d_\rho m_\rho$, while the minimally completed invariant dimension is the same sum. The edge Hilbert-space dimension is $\sum_\rho d_\rho^2$.

Data and code availability

All scripts, source data, numerical results, vector figures and the LaTeX source are supplied with this manuscript. The calculations use deterministic random seeds and require only Python, NumPy, SciPy and Matplotlib.

Competing interests

The authors declare no competing interests.

References

[1] S. W. Hawking. Particle creation by black holes. *Communications in Mathematical Physics*, 43: 199–220, 1975.

[2] Geoffrey Penington. Entanglement wedge reconstruction and the information paradox. *Journal of High Energy Physics*, 2020:2, 2020.

[3] Ahmed Almheiri, Raghu Mahajan, Juan Maldacena, and Ying Zhao. The page curve of hawking radiation from semiclassical geometry. *Journal of High Energy Physics*, 2020:149, 2020.

[4] Ahmed Almheiri, Thomas Hartman, Juan Maldacena, Edgar Shaghoulian, and Amirhossein Tajdini. Replica wormholes and the entropy of hawking radiation. *Journal of High Energy Physics*, 2020:13, 2020.

[5] Chong-Sun Chu. A matrix model proposal for quantum gravity and the quantum mechanics of black holes. *arXiv:2406.01466*, 2024. v3, 2025.

[6] Chong-Sun Chu. Hawking radiation from tunneling in black hole quantum mechanics. *arXiv:2603.12199*, 2026.

[7] Chong-Sun Chu. Quantum horizon and quantum membrane paradigm from black hole quantum mechanics. *arXiv:2607.10561*, 2026.

[8] Roger Howe. Remarks on classical invariant theory. *Transactions of the American Mathematical Society*, 313:539–570, 1989.

[9] William Fulton and Joe Harris. *Representation Theory: A First Course*. Springer, 1991.

[10] Olaf Dreyer, Fotini Markopoulou, and Lee Smolin. Symmetry and entropy of black hole horizons. *Nucl. Phys. B*, 744:1–13, 2006. doi: 10.1016/j.nuclphysb.2006.03.002.

[11] I. M. Gelfand and M. L. Tsetlin. Finite-dimensional representations of the group of unimodular matrices. *Doklady Akademii Nauk SSSR*, 71:825–828, 1950.

[12] Denes Petz. Sufficient subalgebras and the relative entropy of states of a von neumann algebra. *Communications in Mathematical Physics*, 105:123–131, 1986.

[13] William Donnelly and Laurent Freidel. Local subsystems in gauge theory and gravity. *Journal of High Energy Physics*, 2016:102, 2016.

[14] Horacio Casini, Marina Huerta, and Jose Alejandro Rosabal. Remarks on entanglement entropy for gauge fields. *Physical Review D*, 89:085012, 2014.

Extended Data

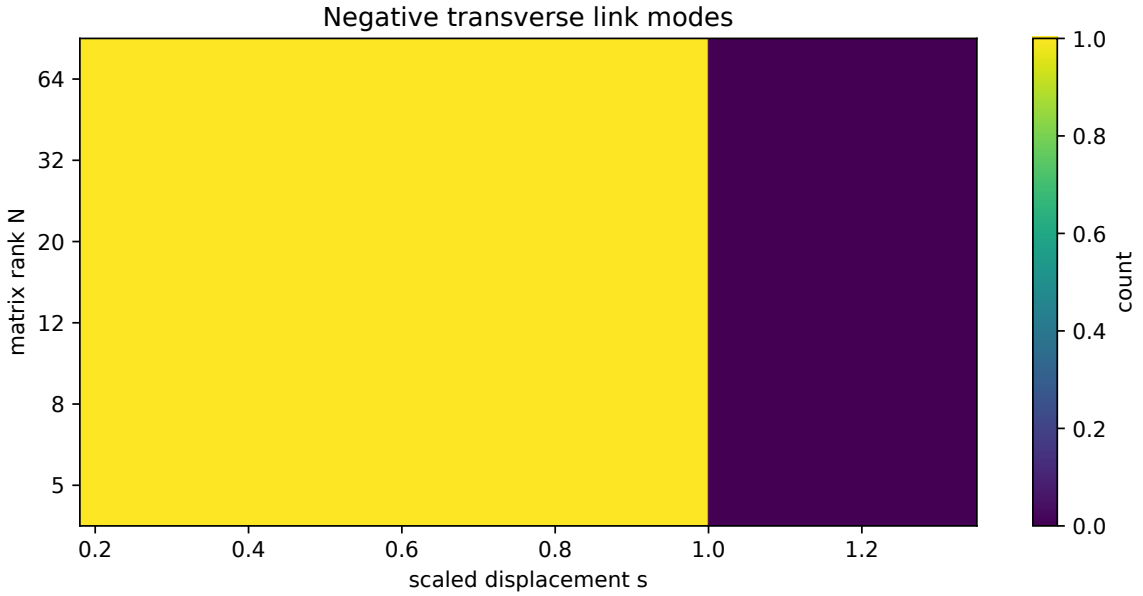


Figure 5: **Extended Data Fig. 1 | Negative-mode count.** The background-covariant transverse Hessian has one negative mode throughout the tachyonic interval for every scanned rank $N \geq 5$ and none after the endpoint $s = 1$.

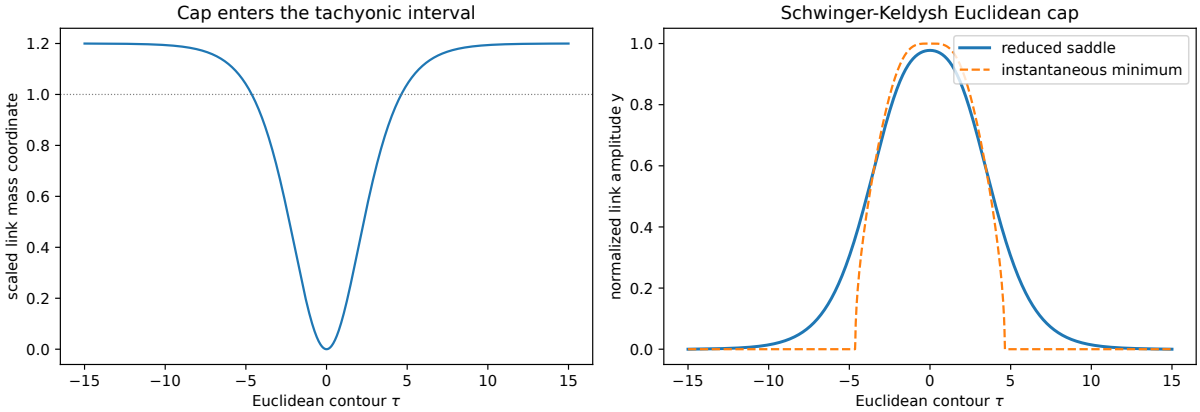


Figure 6: **Extended Data Fig. 2 | Reduced Euclidean link cap.** The prescribed contour enters the unstable interval and nucleates a localized link condensate. The exact saddle is smoothed relative to the instantaneous minimum near the gap-closing points.

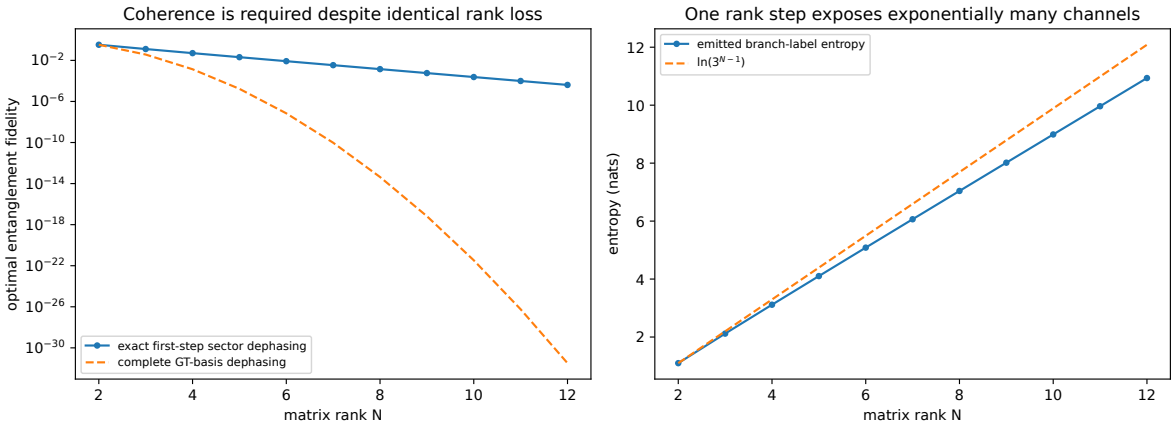


Figure 7: **Extended Data Fig. 3 | Exact branching and dephasing.** One elementary rank loss exposes 3^{N-1} daughter representations. Dephasing their shared label suppresses optimal recovery rapidly, while complete GT-basis dephasing is exponentially stronger.

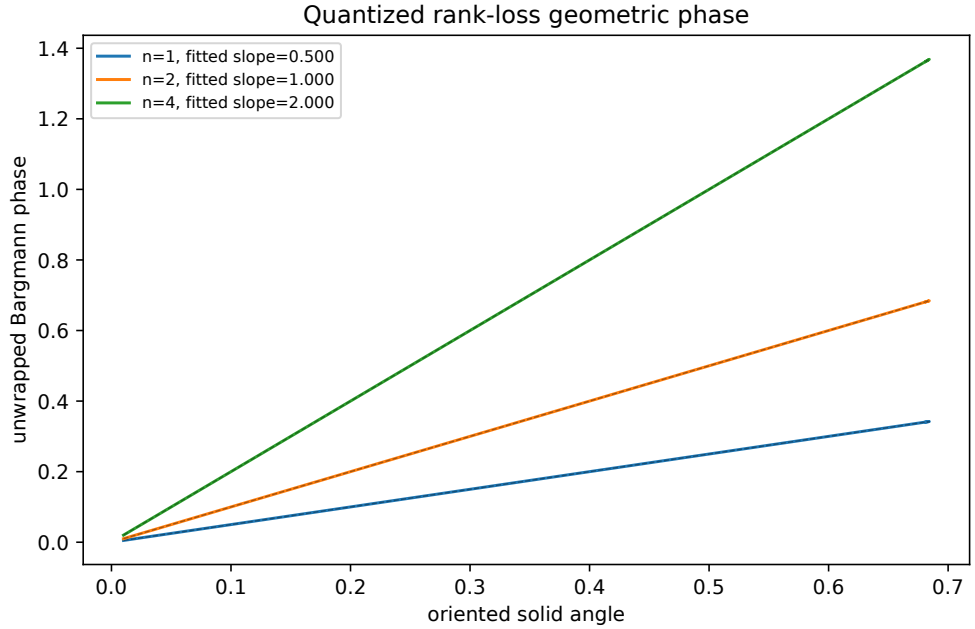


Figure 8: **Extended Data Fig. 4 | Rank-difference geometric phase.** The scalar parent–daughter quotient bundle has Bargmann phase $n\Omega/2$ for rank loss n. The full emitted spinor amplitude can add the known zero-mode spinorial offset and must be fixed by the microscopic detector coupling.

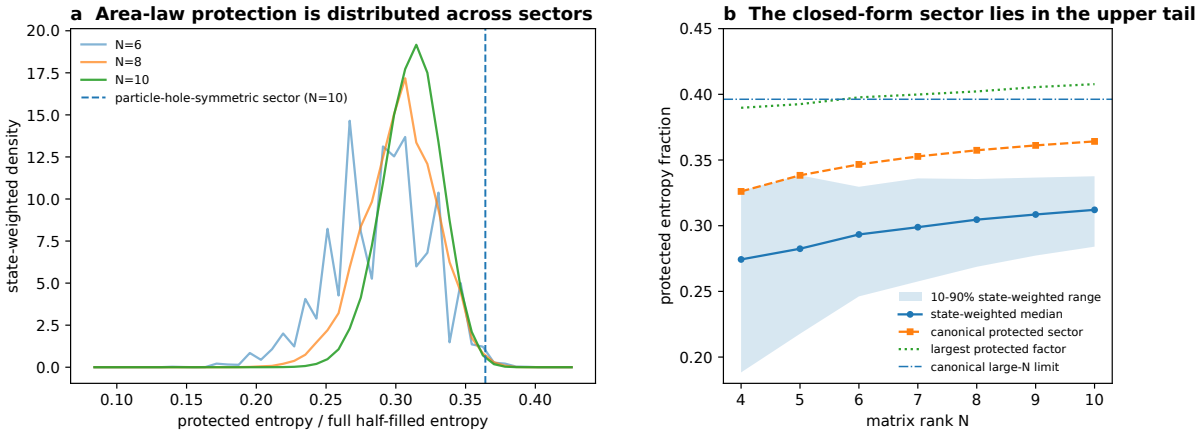


Figure 9: **Extended Data Fig. 5 | Exact census of protected sectors. a**, state-count-weighted distributions of protected entropy across all allowed skew–Howe sectors. **b**, the state-weighted median and 10–90% interval, the self-complementary sector and the largest protected factor. Enumeration is exact through $N = 10$ and the summed sector dimensions reproduce the full half-filled code.

Supplementary Files

This is a list of supplementary files associated with this preprint. Click to download.

- Blackholehawkingsupplement.pdf